

Influence of test charge and uniform magnetic field on charged fluid equilibrium structures

Audrey Trova^{*} and Eva Hackmann

Center of Applied Space Technology and Microgravity (ZARM), University of Bremen, 28359 Bremen, Germany

Vladimír Karas and Kris Schroyen

Astronomical Institute, Academy of Sciences, Boční II, 141 31 Prague, Czech Republic

Jiří Kovář and Petr Slaný

Research Centre for Theoretical Physics and Astrophysics, Institute of Physics, Silesian University in Opava, Bezručovo nám. 13, 746 01 Opava, Czech Republic



(Received 17 January 2020; accepted 10 April 2020; published 22 April 2020)

Equilibrium configurations of a circling electrically charged fluid surrounding a central static black hole endowed with a test electric charge and embedded in a large-scale asymptotically uniform magnetic field are presented. Various configurations of the fluid are influenced by the balance between the gravitational and electromagnetic actions; previous studies of the circling charged fluid configurations around a rotating black hole showed a strong dependence on the spin of the black hole. In this work, we focus on configurations centered in the equatorial plane taking shapes of single or double toroidal structures. Our interest is the existence of these structures, and how various actions, such as electromagnetic, gravitational and centrifugal, influence their shapes and physics.

DOI: [10.1103/PhysRevD.101.083027](https://doi.org/10.1103/PhysRevD.101.083027)

I. INTRODUCTION

The investigation of equilibrium in the toroidal configurations of uncharged or charged fluids is important to understand the structures of accretion disks. Matter in such objects is generally modeled by a fluid approach [1–3]. Accretion disks are inferred to exist in objects of very different scales in the universe, from kilometer to parsec scale, and then appear in various domains. Our interest is about accretion disk orbiting around a black hole as exhibits AGN, quasars or x-ray binaries [4,5]. These objects are the most powerful and efficient stationary engines known in the universe. Here, we are interested in thick accretion disks, especially in those with negligible mass accretion rate, which can be well modeled by toroidal equilibrium configurations of fluids.

Many different studies have been devoted to the uncharged fluid in various spacetimes, from the standard Schwarzschild and Kerr ones, [6–8] to more specific ones [9–12]. In those models, gravity plays a key role in toroidal fluid configurations. However, we know that the magnetic field is also present during the accretion process and can influence the accretion of the fluid. Studies about magnetized tori have been performed, by adding a purely toroidal

magnetic field attached to the fluid [13,14], and by including the effect of self-gravity [15]. In this respect, interests in charged fluid arise. Electric charges can be developed by various mechanisms, for instance, in AGN, dusty tori are charged by strong irradiation by x-rays from the central sources [16] or charge exchange in plasmas [17,18]. The magnetic field can be produced either by the central object, by the fluid itself, or by an external source of matter as a large-scale organized magnetic field. That kind of field can occur in the vicinity of magnetic star or magnetar [19].

Therefore, an extension of the Polish doughnut model [6,7] has been introduced [20–24] based on an addition of a global nonzero charge to the circling fluid, consequently interacting with a background electromagnetic field of external origin, or with the one coupled to the central object [25]. Along with this series of papers, it was shown that bound fluid structures in the equatorial plane exist in various spacetimes and under the influence of external electromagnetic forces. Also, unique structures on the polar axis, named “polar clouds,” have been found only orbiting around a charged black hole embedded in an external magnetic field. These structures can scatter and polarize light on the axis and they can only orbit in rigid rotation. Following that result, we showed that the rotation of the central black hole can replace the effect of one of the two

^{*}audrey.trova@zarm.uni-bremen.de

external forces and can allow the existence of polar clouds. Besides that polar solutions, we worked on off-equatorial tori, meaning “levitating” structures above the equatorial plane, which can only exist with a constant angular momentum rotation law. The presence of the electromagnetic field is also a necessary condition of their existence. These structures can be seen as diluted halos and can play the role of coroneae. Then, we can study configurations of charged fluids around uncharged or charged, and static or rotating, black holes or other compact objects surrounded by magnetic fields. Note that even if astrophysical black holes are thought to be quickly neutralized by the accretion of opposite charge of the fluid, a small net equilibrium charge remains [28,29]. That small charge can still influence the charged fluid motion in the ambient electromagnetic field. Besides, some of the models take into account the self field produced by the circling fluid (gravitational and electromagnetic) [26,30–32].

Here, we apply the model introduced and discussed in the series of papers [20–24,33] to the case of static charged black hole immersed in an external asymptotically uniform magnetic field. The constructed stationary structures give us an insight into how mass and charge are distributed within the disk, which may be taken as an initial step toward dynamical studies. We aim to understand how the combination of other forces like the magnetic and electric ones influence the shape and the mass and charge distributions of such structures. We consider a charged fluid approach with no internal viscosity and heat conduction (the perfect fluid approach). The field produced by the charged black hole and the ambient magnetic field are test fields and do not influence the spacetime. The fluid is studied in a spherically symmetric gravitational field described by the Schwarzschild metric, where it circles with a constant specific angular momentum, in contrast to related earlier studies that used a constant angular velocity instead. Moreover, the fluid has zero conductivity, then the charges are adhered to the fluid particles, and they are carried convectively. This approach is the opposite scenario of the ideal magnetohydrodynamics, where the conductivity is infinite. This opposite concept was first developed in [20] on the background of Reissner-Nordström black hole. The electromagnetic field produced by the charged fluid is neglected compared to the external ones. To achieve this goal we start in Sec. II by introducing the model. We describe the general equations, the assumptions, and the background fields. In Sec. III, we give the expression of the effective potential which leads to the equipotential surfaces. The following Sec. IV is devoted to the conditions of existence of the equilibrium structures. We show how to choose the set of parameters in a way to reach a bound fluid configuration. This leads to the construction of the solutions in Sec. V for different sets of parameters. Finally, in Sec. VI, we discuss the influence of the test charge and test magnetic field on the solutions.

II. EQUILIBRIUM CONFIGURATIONS—THE MODEL

A. General equations and assumptions

Within the general relativistic approach, thick accretion disks with negligible accretion flow can be modeled by circling fluids, being described by the conservation laws and Maxwell equations

$$\nabla_{\beta} T^{\alpha\beta} = 0, \quad (1)$$

$$\nabla_{\beta} F^{\alpha\beta} = 4\pi J^{\alpha}, \quad (2)$$

$$\nabla_{(\gamma} F_{\mu\nu)} = 0. \quad (3)$$

Neglecting the viscosity of the fluid and the heat conduction, the proper energy-momentum tensor can be written as $T^{\alpha\beta} = T_{\text{PF}}^{\alpha\beta} + T_{\text{EM}}^{\alpha\beta}$, where its perfect fluid and electromagnetic parts are expressed as

$$T_{\text{PF}}^{\alpha\beta} = (\epsilon + p)U^{\alpha}U^{\beta} + pg^{\alpha\beta}, \quad (4)$$

$$T_{\text{EM}}^{\alpha\beta} = \frac{1}{4\pi} \left(F^{\alpha}_{\gamma} F^{\beta\gamma} - \frac{1}{4} F_{\gamma\delta} F^{\gamma\delta} g^{\alpha\beta} \right), \quad (5)$$

and p is the pressure in the fluid, ϵ the energy density, and U^{α} the four-velocity field of the fluid.

The electromagnetic field $F^{\alpha\beta}$ can be split into two terms: the tensor describing external electromagnetic forces acting on the fluid, $F_{\text{EXT}}^{\alpha\beta}$, and the tensor describing self-electromagnetic interactions due to charged particles in the fluid, $F_{\text{SELF}}^{\alpha\beta}$. In the following, since we neglect the self-electromagnetic interactions (considering them to be relatively weak), we have $F_{\text{SELF}}^{\alpha\beta} \ll F_{\text{EXT}}^{\alpha\beta}$. This means that the electromagnetic field produced by the fluid itself does not contribute neither to the given gravitational field, i.e., the spacetime geometry $g_{\alpha\beta}$, nor to the given external electromagnetic field $F_{\text{SELF}}^{\alpha\beta}$; similarly, we expect the given gravitational field not to be affected by the fluid gravitational self-field—the fluid is considered to be fully the test one. The external electromagnetic field $F_{\text{EXT}}^{\alpha\beta}$ can be expressed as

$$F_{\text{EXT}}^{\alpha\beta} = g^{\alpha\mu} g^{\beta\nu} (\nabla_{\mu} A_{\nu} - \nabla_{\nu} A_{\mu}), \quad (6)$$

where A_{ν} is the external electromagnetic field four-potential. Depending on the charge density q , electric conductivity σ , and on the four-velocity field U^{α} , the four-current density field J^{α} is given by Ohm’s law

$$J^{\alpha} = qU^{\alpha} + \sigma F^{\alpha\beta} U_{\beta}. \quad (7)$$

By using Eqs. (1), (2), (3), the energy-momentum tensor decomposition, and the test fluid assumption, we get the “master formula,”

$$\nabla_\nu T_{\text{PF}}^{\alpha\beta} = F_{\text{EXT}}^{\alpha\beta} J_\nu, \quad (8)$$

for the charged fluid moving in the given fields.

In our model, we presume the charged fluid to stationary circle in the azimuthal direction of the given electromagnetic $F_{\text{EXT}}^{\alpha\beta}$ and gravitational $g_{\alpha\beta}$ fields, both stationary and axially symmetric. Thus, in the used Boyer-Linquist coordinates (t, r, θ, ϕ) , we have the four-velocity field of the fluid $U^\alpha = (U^t, 0, 0, U^\phi)$, the electromagnetic field four-potential $A_\mu = (A_t, 0, 0, A_\phi)$, and, especially, $J^\alpha = (J^t, 0, 0, J^\phi)$. It means, the fluid conductivity factor of the fluid $\sigma = 0$; this is the complete opposite of the ideal magnetohydrodynamics, where the conductivity is infinite. Our assumptions say that the charges are stuck to the fluid elements and follow their rotation. Putting a nonzero finite conductivity could lead to a nonazimuthal current determined by the term $\sigma F^{\alpha\beta} U_\beta$, which can have nonazimuthal component for $\beta = \phi$. This would be inconsistent with the assumption of the pure azimuthal circular motion of whole the fluid, governed by substantial gravitational and electromagnetic ‘‘Lorentz’’ actions.

Under the mentioned conditions, the master formula (8) gives us the set of partial differential equations for the fluid,

$$\begin{aligned} \partial_r w &= -\partial_r \ln |U_t| + \frac{\Omega \partial_r \ell}{1 - \Omega \ell} + \frac{q}{p + \epsilon} (U^t \partial_r A_t + U^\phi \partial_r A_\phi), \\ \partial_\theta w &= -\partial_\theta \ln |U_t| + \frac{\Omega \partial_\theta \ell}{1 - \Omega \ell} + \frac{q}{p + \epsilon} (U^t \partial_\theta A_t + U^\phi \partial_\theta A_\phi), \end{aligned} \quad (9)$$

the so-called ‘‘transformed pressure equations,’’ where w is the pressure (enthalpy) function defined as $\partial_\mu w = \frac{\partial_\mu p}{p + \epsilon}$, $\mu = (r, \theta)$. ρ, q, p are respectively the mass density, the charge density and the pressure of the fluid. The specific angular momentum, $\ell = -U_\phi / U_t$, and the angular velocity, $\Omega = U^\phi / U^t$, are related by the formula

$$\Omega = -\frac{\ell g_{tt} + g_{t\phi}}{\ell g_{t\phi} + g_{\phi\phi}}, \quad (10)$$

and by using the normalization condition, we can derive the t -component of the four-velocity field

$$(U_t)^2 = \frac{g_{t\phi}^2 - g_{tt} g_{\phi\phi}}{\ell^2 g_{tt} + 2\ell g_{t\phi} + g_{\phi\phi}}. \quad (11)$$

B. Background fields

As the background for the circling fluid, we consider Schwarzschild black hole spacetime, in the dimensionless system of units described by the line element

$$ds^2 = g_{tt} dt^2 + g_{rr} dr^2 + g_{\theta\theta} d\theta^2 + g_{\phi\phi} d\phi^2, \quad (12)$$

with the metric coefficients

$$\begin{aligned} g_{tt} &= -\left(1 - \frac{2}{r}\right), & g_{rr} &= \left(1 - \frac{2}{r}\right)^{-1}, \\ g_{\theta\theta} &= r^2, & g_{\phi\phi} &= r^2 \sin^2 \theta. \end{aligned} \quad (13)$$

The spacetime is then accompanied by a test asymptotically uniform magnetic field (aligned with the $\theta = 0$ axis) given in terms of the four-potential components [28]

$$A_t = -\frac{Q}{r}, \quad A_\phi = \frac{B}{2} r^2 \sin^2 \theta, \quad (14)$$

where B and Q are the strength of the magnetic field and the test charge of the black hole.

Note that for $g_{tt} < 0$ of the Schwarzschild spacetime, i.e., above the event horizon ($r > 2$), the condition $\ell^2 g_{tt} + g_{\phi\phi} > 0$ must be fulfilled to maintain $(U_t)^2 > 0$. This is the case when

$$\ell^2 < \frac{r^3 \sin^2 \theta}{r - 2} \equiv \ell_{\text{ph}}^2(r, \theta). \quad (15)$$

In the equatorial plane ($\theta = \pi/2$), the function $\ell_{\text{ph}}^2(r)$ governs the photon motion. The minimum of the function $\ell_{\text{ph}}^2(r)$, corresponding to the values $r = 3$ and $\ell^2 = 27$, represents the location and impact parameter of the circular photon orbit. Any geodesic that crosses the photon sphere from the outside is going to spiral into the black hole.

III. EFFECTIVE POTENTIAL

In static spacetimes, where there is $U^t = g^{tt} U_t$ and $U^\phi = g^{\phi\phi} U_\phi$, the set of transformed pressure equations (9) takes the form

$$\begin{aligned} \partial_r w &= -\partial_r \ln |U_t| + \frac{\Omega \partial_r \ell}{1 - \Omega \ell} + \frac{q U_t}{p + \epsilon} \mathcal{R}, \\ \partial_\theta w &= -\partial_\theta \ln |U_t| + \frac{\Omega \partial_\theta \ell}{1 - \Omega \ell} + \frac{q U_t}{p + \epsilon} \mathcal{T}, \end{aligned} \quad (16)$$

where we briefly denote the radial and latitudinal electromagnetic terms as $\mathcal{R} = g^{tt} \partial_r A_t - \ell g^{\phi\phi} \partial_r A_\phi$ and $\mathcal{T} = g^{tt} \partial_\theta A_t - \ell g^{\phi\phi} \partial_\theta A_\phi$. In general, all the solutions of this set of equations are subjected to the integrability condition

$$\partial_r \partial_\theta w = \partial_\theta \partial_r w, \quad (17)$$

which must be considered simultaneously.

Particularly, considering the transformed pressure equations (16), and choosing the fluid circulation so that $\ell = \text{const}$, the integrability condition (17) reads

$$\partial_\theta \left(\frac{qU_t}{p+\epsilon} \mathcal{R} \right) = \partial_r \left(\frac{qU_t}{p+\epsilon} \mathcal{T} \right). \quad (18)$$

In the background given by the metric coefficients (13) and by the four-potential (14), the electromagnetic terms take the form

$$\mathcal{R} = -\frac{Q}{r(r-2)} + \ell \frac{B}{r}, \quad \mathcal{T} = \ell B \frac{\cos \theta}{\sin \theta}, \quad (19)$$

which can be conveniently written as

$$\mathcal{R} = \partial_r S, \quad \mathcal{T} = \partial_\theta S, \quad (20)$$

where $S = S_1 B$, $S_1 = [-\frac{\epsilon}{2} \ln(\frac{r-2}{r}) - \ell \ln(r \sin \theta)]$ and $e = Q/B$. Thus, the integrability condition (18), now written in the form

$$\partial_\theta \left(\frac{qU_t}{p+\epsilon} \partial_r S \right) = \partial_r \left(\frac{qU_t}{p+\epsilon} \partial_\theta S \right), \quad (21)$$

is perfectly fulfilled when we chose $\frac{qU_t}{p+\epsilon} = f(S)$.

Consequently, the set of transformed pressure equations (16) can be rewritten as

$$\begin{aligned} \partial_r w &= \frac{\partial_r p}{p+\epsilon} = -\partial_r \ln |U_t| + f(S) \partial_r S, \\ \partial_\theta w &= \frac{\partial_\theta p}{p+\epsilon} = -\partial_\theta \ln |U_t| + f(S) \partial_\theta S, \end{aligned} \quad (22)$$

with its solution $w = \int_0^p \frac{dp}{p+\epsilon}$ expressed in the closed form

$$\begin{aligned} w(r, \theta) &= -W(r, \theta) + W^{\text{in}} \\ &= -\ln \left| \frac{U_t}{U_t^{\text{in}}} \right| + \int_{S^{\text{in}}}^S f(S) dS, \end{aligned} \quad (23)$$

if the fluid equation of state takes the form $p = p(\epsilon)$.

Here, we define $W(r, \theta)$ as the effective potential, and denote W^{in} as the integration constant, used as an offset to choose the radial extension of the bound fluid configuration. The function f is an arbitrary function linked to the charge density of the torus. To keep consistency with our previous works, we choose a power law $f(S) = \mu_n S^n$ for its specification, whereas the constant μ_n represents the fluid charge scaling factor. Thus, the effective potential (23) can be written in the form

$$W(r, \theta) = \ln |U_t| - k_0 \frac{S_1^{n+1}}{n+1}, \quad (24)$$

where $k_0 = \mu_n B^{n+1}$ and $U_t^2 = \frac{-g_{tt} g_{\phi\phi}}{\ell^2 g_{tt} + g_{\phi\phi}}$; for $n = 1$, we get the particular form

$$W(r, \theta) = \frac{1}{2} \ln \frac{-g_{tt} g_{\phi\phi}}{\ell^2 g_{tt} + g_{\phi\phi}} - k_0 \frac{S_1^2}{2}. \quad (25)$$

IV. CONDITIONS OF EXISTENCE OF EQUILIBRIUM STRUCTURES

A. Mathematical conditions

The conditions of existence of a bound fluid structure is linked to the existence of a pressure maximum (maximum of the enthalpy, minimum of the effective potential). We are going to work with the effective potential. By setting the coordinates of the minimum of W (r_c, θ_c), the necessary conditions for a minimum read

$$\partial_r W|_{r=r_c, \theta=\theta_c} = 0, \quad (26a)$$

$$\partial_\theta W|_{r=r_c, \theta=\theta_c} = 0, \quad (26b)$$

while the sufficient ones require in addition

$$\partial_{rr}^2 W|_{r=r_c, \theta=\theta_c} > 0, \quad (27a)$$

$$\det \mathcal{H}|_{r=r_c, \theta=\theta_c} > 0, \quad (27b)$$

where \mathcal{H} is the Hessian matrix,

$$\mathcal{H} = \begin{pmatrix} \partial_{rr}^2 W & \partial_{r\theta}^2 W \\ \partial_{\theta r}^2 W & \partial_{\theta\theta}^2 W \end{pmatrix}. \quad (28)$$

Particularly, in this work, we are interested in configurations in the equatorial plane ($\theta_c = \pi/2$). In that case, the cross derivatives vanish, thus condition (27b) reduces to

$$\partial_{\theta\theta}^2 W|_{r=r_c, \theta=\theta_c} > 0. \quad (29)$$

B. Relation between k_0 and ℓ

In the case where the center of the bound structure lies in the equatorial plane, the second necessary condition is automatically fulfilled and the first condition can be fulfilled by setting

$$k_0 = \frac{[2(r_c - 2)^2 \ell^2 - r_c^3] (e \ln \frac{r_c - 2}{r_c} + 2\ell \ln r_c)^{-1}}{((r_c - 2)\ell^2 - r_c^3)(e - \ell(r_c - 2))}. \quad (30)$$

Our system is characterized by five parameters: ℓ, e, n, r_c and k_0 . Equation (26a) and the two inequations in (27) give

restrictions to the range of possible values for these parameters.

We reduce the discussion to the case $n = 1$. While k_0 is determined by satisfying Eq. (26a) [see Eq. (30)], one of the remaining parameters (in this discussion we chose ℓ) is restricted to certain values depending on the choice of the remaining parameters. The restriction on the choice of ℓ will be evaluated depending on k_0 —and therefore [according to Eq. (30)] on r_c —for a prescribed value of e in terms of bifurcation sets. To do so, we use catastrophe theory (branch of bifurcation theory in the study of dynamical systems) and, in particular, the cusp catastrophe [34–38]. It is used to study critical points of a potential. At these points, not only the first derivative but also higher derivatives of the potential become zero. Small changes in the value of one of the potential parameters will cause stationary points (minima or maxima in the potential) to appear or disappear. In the case of $W(r, \theta)$, the critical points are given by

$$\partial_r W(r_c, \theta_c) = 0, \quad (31)$$

$$\partial_r^2 W(r_c, \theta_c) = 0. \quad (32)$$

The bifurcation set consists of the parameter pairs (k_0, ℓ) of all critical points of $W(r, \theta)$, for $n = 1$ and a fixed value of e . An exemplary bifurcation set is shown in Fig. 1, for $n = 1$ and some fixed value of e . The bifurcation set allows us to discuss the range of values for ℓ and k_0 for which bound charged fluid structures can be found for a given value of e . Due to the symmetry $W(e, \ell) = W(-e, -\ell)$, the following discussion is restricted to $\ell > 0$.

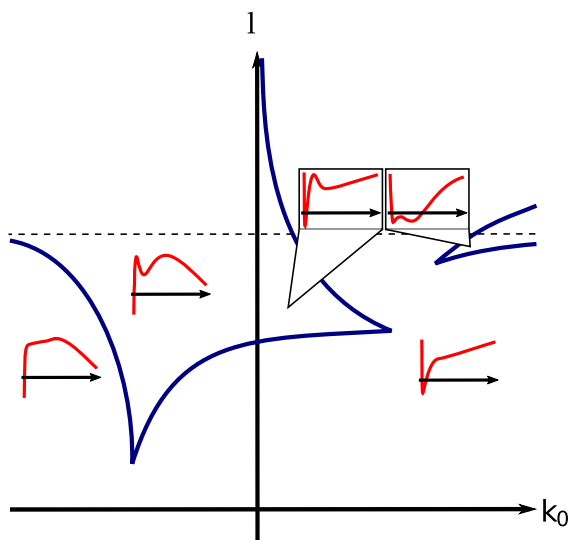


FIG. 1. The blue curve depicts a typical structure of the bifurcation set for $n = 1$ in the (k_0, ℓ) -control space (the blue curve contains all extremal points of $W(r, \theta)$ for which $\partial_r^2 W = 0$ is satisfied).

By its definition the bifurcation set divides the control space into two different areas, whose corresponding potentials $W(r, \frac{\theta}{2})$ show a different number of one or otherwise three extrema. $W(r, \theta)$ shows the following behavior:

- (i) for $k_0 > 0$, $W_{r \rightarrow 2, \infty}(r, \theta_c) \rightarrow -\infty$,
- (ii) for $k_0 < 0$, $W_{r \rightarrow 2, \infty}(r, \theta_c) \rightarrow +\infty$.

The case $k_0 = 0$ describes the uncharged case. This leads to a total of one to two minima and no or one maximum for $k_0 < 0$ and no or one minimum and one or two maxima for $k_0 > 0$, in the effective potential. The qualitative structure of $W(r, \theta_c)$ for a (k_0, ℓ) parameter set from the different areas of the control space is shown in Fig. 1. Local minima mark the center of a possible bound structure solutions, maxima correspond to possible inner and outer cusp points. For these points, to form actual centers of bound structure solutions (representing the thick accretion disk), the second sufficient condition $\partial_{\theta\theta}^2 W > 0$ has to be fulfilled at these points as well. We will discuss that condition later in this section. If the bound fluid structure ends at a cusp point, the matter is expected to flow out of the structure at this point. Then, it might either be accreted by the central object (in case of an inner cusp, where the corresponding maximum is located at a radius smaller than the center of the fluid structure) or it can flow away from the central object (in case of an outer cusp, where the corresponding maximum is located at bigger radii than the center of the fluid structure). We can see that no outer cusp points are possible except if an inner cusp is also present. Moreover, we can note that for $k_0 < 0$ no inner cusp points exist, while they do for $k_0 > 0$. As mentioned above, the system is also depending on e , the ratio of the test charge over the test magnetic field. Therefore, the bifurcation set has to change with e . Figures 2 and 3 depict the bifurcation set for several positive and negative values of e for $n = 1$ in the control space (k_0, ℓ) . One can see that the behavior of the potential changes with e , meaning that the equilibrium structure is influenced by the charge and the magnetic field of the background. Moreover, for each value of e , all the bifurcation sets cross in $(k_0 = 0, \ell = \sqrt{13.5})$. This point corresponds to the specific angular momentum of an uncharged test particle moving along the marginally stable circular orbit (ISCO). In Fig. 4 the special case of $e = 350$ is shown, where a new area is formed. The cusp shown in the right plots in Figs. 2 and 3 comes to cross the bifurcation set in the left plots. In this particular space, the potential should exhibit three maxima and two minima. As we said, these minima points can be centers of bound structure solutions if the second sufficient condition $\partial_{\theta\theta}^2 W > 0$ is fulfilled. This is plotted in Fig. 5 for positive values of e . Three area appears, where solutions are possible:

- (i) area I shrinks for larger values of e (indicated by lightening up the blue coloring) in $\Delta e = 2$ steps from $e = 1$ (darkest blue color) up to $e = 19$ (lightest blue color),

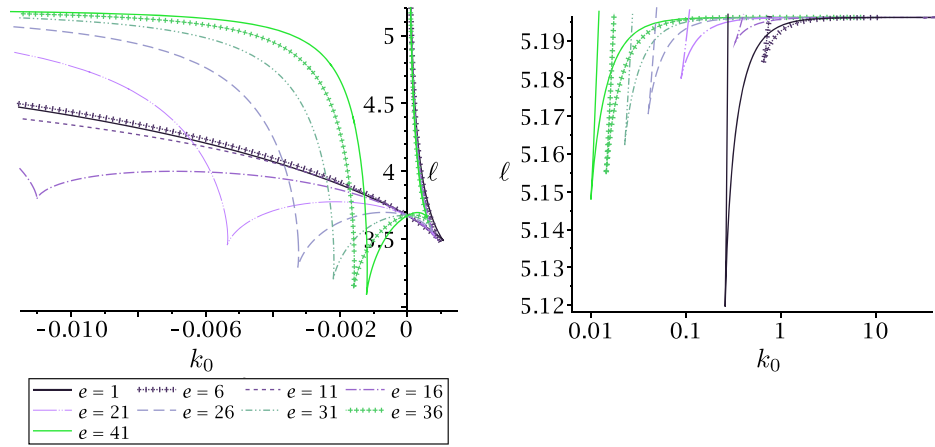


FIG. 2. Bifurcation set for $n = 1$ for various values of e . The qualitative structure of $W(r, \theta_c)$ can be read from the plots as described in Fig. 1.

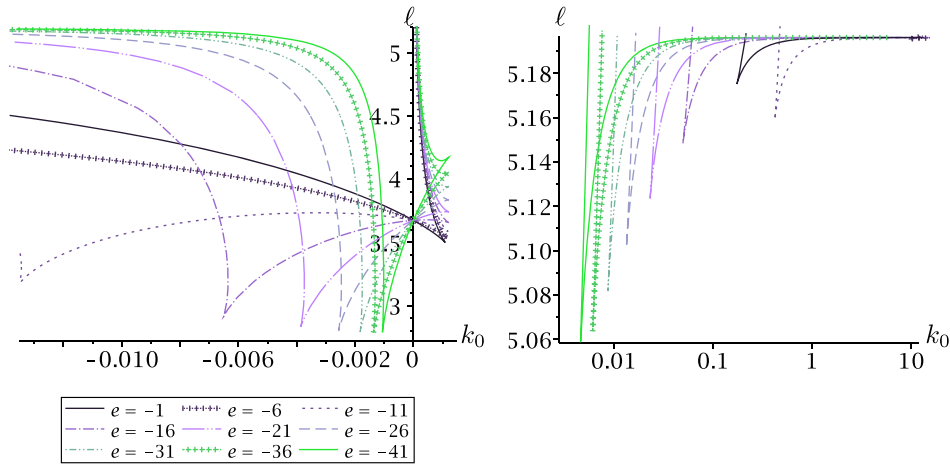


FIG. 3. Bifurcation set for $n = 1$ for various values of e . The qualitative structure of $W(r, \theta_c)$ can be read from the plots as described in Fig. 1.

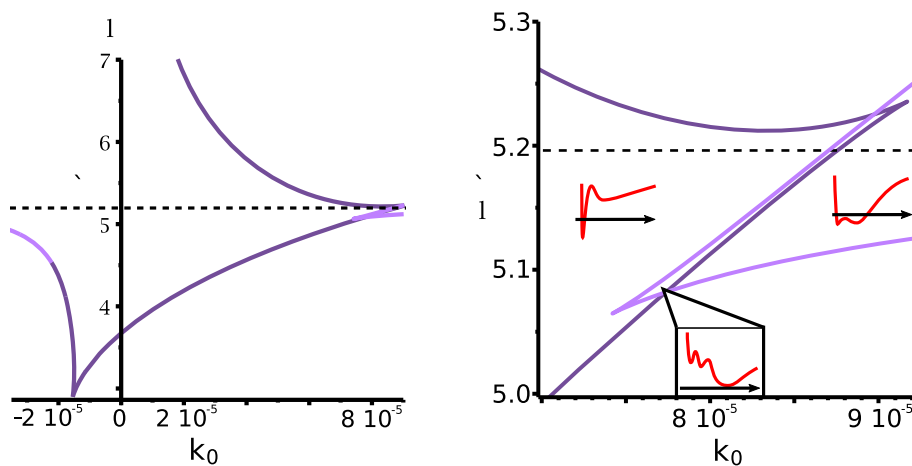


FIG. 4. Bifurcation set for $n = 1$ and $e = 350$. Two cusps overlap in the bifurcation set. This leads to a potential structure of $W(r, \theta_c)$ with two minima and three maxima for a parameter set (k_0, ℓ) from the region bordered by the two cusps.

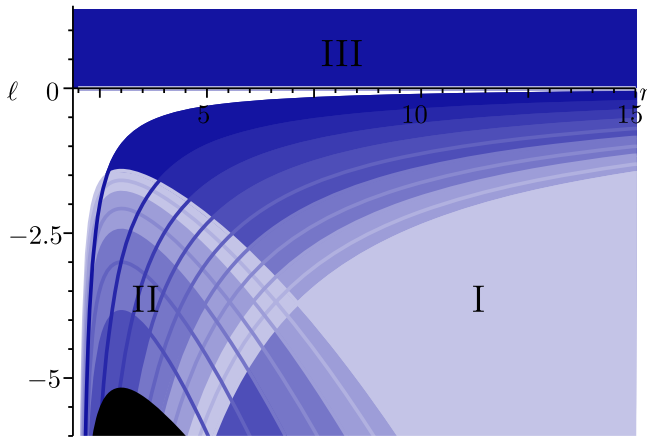


FIG. 5. Map of the extremal points $(r_c, \theta_c = \pi/2)$ of W for different values of e plotted over ℓ . Scaling parameter k_0 (Eq. (30)) is chosen such that necessary conditions $(\partial_r W = 0, \partial_\theta W = 0)$ are satisfied at each point and hence changes throughout the plot. The second sufficient condition of a local minimum in W (meaning $\partial_{\theta\theta}^2 W > 0$) is satisfied for points located in one of the three areas I–III. The black area indicates the region of superluminal motion.

- (ii) area II grows for larger values of e ,
- (iii) area III is solely confined by $\ell > 0$.

The second sufficient condition is therefore always satisfied for $\ell > 0$ for any value of $e > 0$. Due to the symmetry $W(e, \ell) = W(-e, -\ell)$, the plot contains the discussion for negative values of e , simply by flipping the plot along with the r -axis. Every minimum of $W(r, \theta_c)$ corresponds to the existence of a bound fluid structure, while maxima at radii smaller or bigger than r_c might serve as an inner cusp or outer cusp of a bound fluid structure. Here a “double solution” of two bound fluid structures is possible if $W(r, \theta_c)$ possesses two minima. According to Figs 2–4, this is the case for certain choices of $(k_0 < 0, \ell)$, but also for certain $(k_0 > 0, \ell)$ -pairs in case of a sufficiently big value of e (see Fig. 4 for $e = 350$). As we said, at the beginning of this section, another parameter is playing a role, n , the power law of the f -function. While the overall structure of the bifurcation sets does not change for bigger values of n ($n > 1$), it changes significantly for smaller values of n ($n < -1$). However, for very small values of n , the behavior of $W(r, \theta)$ seems to approach that of the uncharged case for a broad range of k_0 . Something comparable can be found for very big values of n , however, the behavior of $W(r \rightarrow \infty, \theta_c)$ changes drastically.

V. EQUILIBRIUM CONFIGURATIONS OF A CHARGED FLUID

In this section, we are going to construct solutions in the equatorial plane by setting the parameter $n = 1$, and choosing the couple (ℓ, k_0) and e according to the kind of solution we want (see Fig. 2). Then we can have:

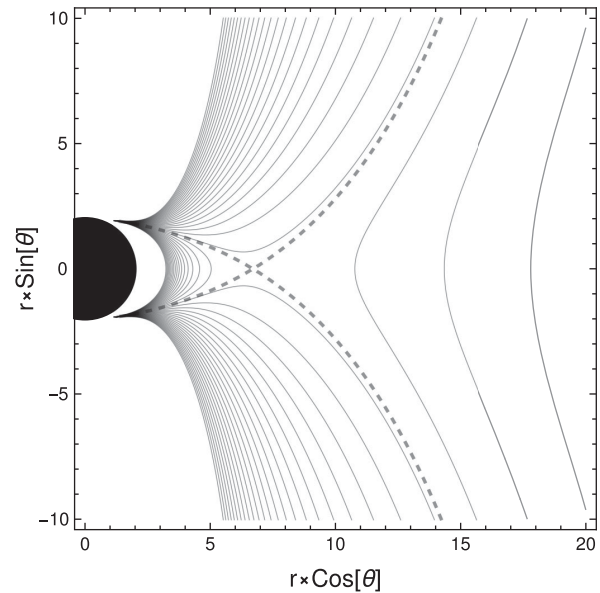


FIG. 6. Map of the equipotential surfaces using the following parameters: $\ell = \sqrt{11}$, $k_0 = 0.002$, and $e = 10$. The dashed line correspond to the equipotential surface of the cusp.

- (i) Structures with a cusp only, for instance, for the following parameters $\ell = \sqrt{11}$, $k_0 = 0.002$ and $e = 10$. This type of solutions is plotted in the Fig. 6.
- (ii) Structures with a bound fluid configuration only, for instance, for $\ell = 3.5$, $k_0 = -0.006$ and $e = 21$. This kind of solutions is shown in the Fig. 7.
- (iii) Finally, we can have solutions with a bound fluid surrounded by an inner and an outer cusps and

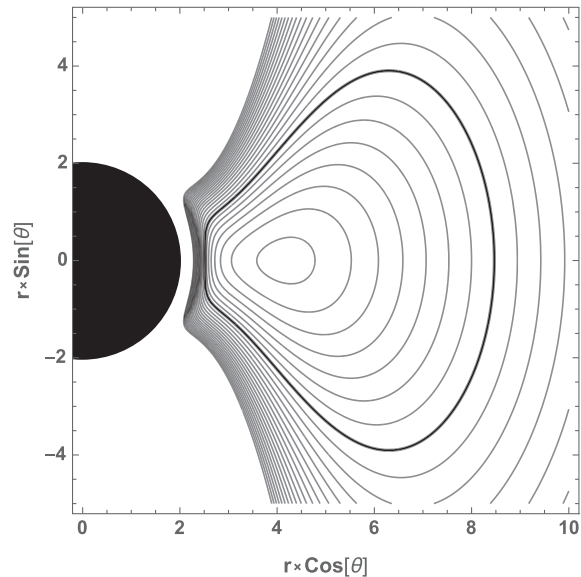


FIG. 7. Map of the equipotential surfaces using the following parameters: $\ell = 3.5$, $k_0 = -0.006$ and $e = 21$. The thick black curve shows a closed equipotential surface, meaning a bound fluid structure. The dashed line corresponds to the equipotential surface of the inner cusp.

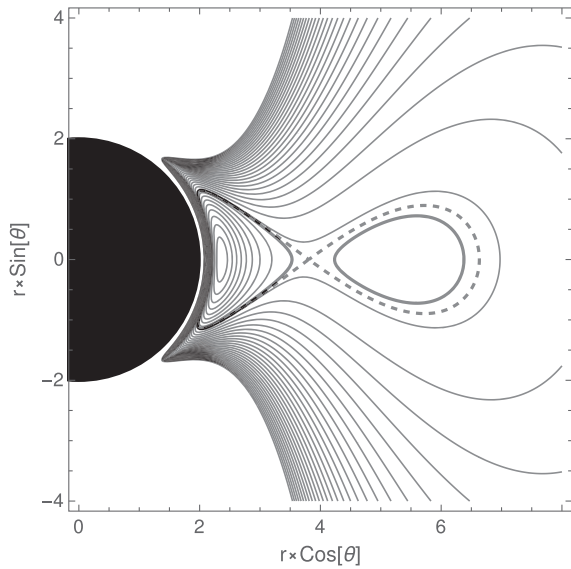


FIG. 8. Map of the equipotential surfaces using the following parameters: $\ell = \sqrt{13.2}$, $k_0 = -0.002$ and $e = 28$. The thick black curve shows two closed equipotential surfaces of same potential value. The dashed line is the equipotential surface of the cusp.

double solutions with two bound fluid structures connected by a cusp. These configurations can be obtained, for instance, for the following set of parameters: $\ell = \sqrt{13.2}$, $k_0 = -0.002$ and $e = 28$, and $\ell = \sqrt{15}$, $k_0 = 0.0001$ and $e = 10$ respectively. They are plotted in Figs. 8, 9 and 10. Even if the assumption of the model is the pure circular and stationary motion, the cusp point can serve as a point

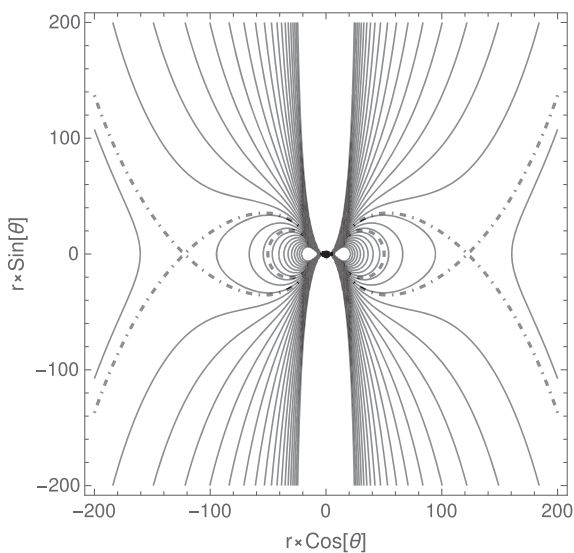


FIG. 9. Map of the equipotential surfaces using the following parameters: $\ell = \sqrt{15}$, $k_0 = 0.0001$, and $e = 10$. The dashed line corresponds to the equipotential surfaces of the inner cusp and the dot dashed line the one of the outer cusp.

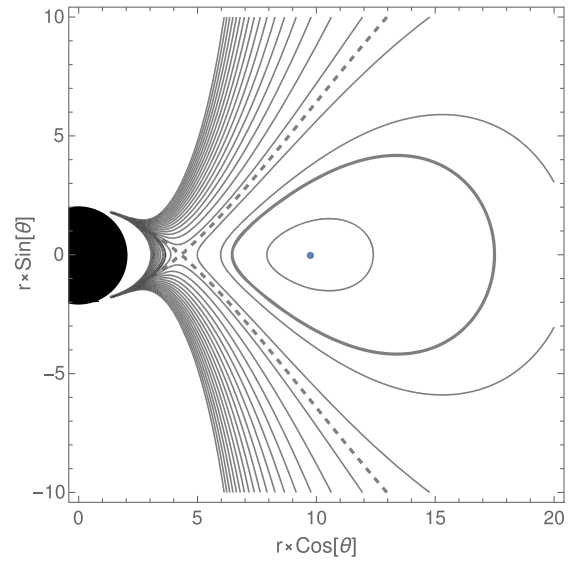


FIG. 10. Zoom of the Fig. 9. The dashed line is the equipotential surface of the inner cusp and the thick curve one of the closed equipotential surface.

where an accretion flow or outflow can occur. If the fluid reaches that point, it will flow out of the bound structure. Note that we cannot find solutions that exhibit an inner cusp alone with a bound structure or an outer cusp alone with a bound fluid structure. An inner cusp is present with an outer cusp and vice versa but only for a special combination of parameters both cusps lie on the same equipotential surfaces. More frequently, the bound structure is surrounded by a critical surface with only one cusp (inner or outer).

It is interesting to see the various configurations that can be constructed within the presented model. Especially, the double cusp and double tori structures. They seem to be always possible when the charge and the magnetic field are present with constant ℓ or with a dipolar magnetic field with constant ℓ or Ω .

VI. INFLUENCE OF CHARGE AND ELECTROMAGNETIC FIELD

A. Vector fields

In this section, we aim to understand the involvement of the various processes in the creation of the double tori solution, as depicted in Fig. 8. As already described in [23], the function $f(S)$ involves the specific charged distribution through the disk. Then, the electromagnetic force will interact with the fluid through the following term $f(S)\partial_\mu S$, $\mu \in \{r, \theta\}$. This term contains one term describing the electric force acting on the charged particles of the fluid, namely $f(S)g^{tt}\partial_\mu A_t$ and another term describing the Lorentz force acting on the charged particles moving in the magnetic field, namely $f(S)g^{\phi\phi}\partial_\mu A_\phi$. Depending on the

value of ℓ , both terms can result in an attractive or repulsive force. We can plot, the strength of the different terms for certain configurations to understand the impact of the processes involved.

In Fig. 11, we plot the different vector fields corresponding to the different terms of the pressure equation.

- (i) As expected, all the arrows in Fig. 11(d) point the direction of the pressure maximum.
- (ii) We can see that both the fields of the magnetic and electric forces change signs through the fluid.
- (iii) As expected, the field due to the magnetic force is only in the R – direction. As the magnetic field is uniform in the vertical direction, this result is coherent.

We can assume, regarding the four plots that, the extended shape in the outer region should be due to the electric force which is dominant here. On the other hand, close to the inner edge, the effect of the electric force decreases and is balanced by the acceleration. The same study is done for another interesting configuration, the double tori structure (see Fig. 12). We can see that a change of sign happens for both the electric and magnetic parts. It is close to the second pressure maximum. As expected, the vector of the total

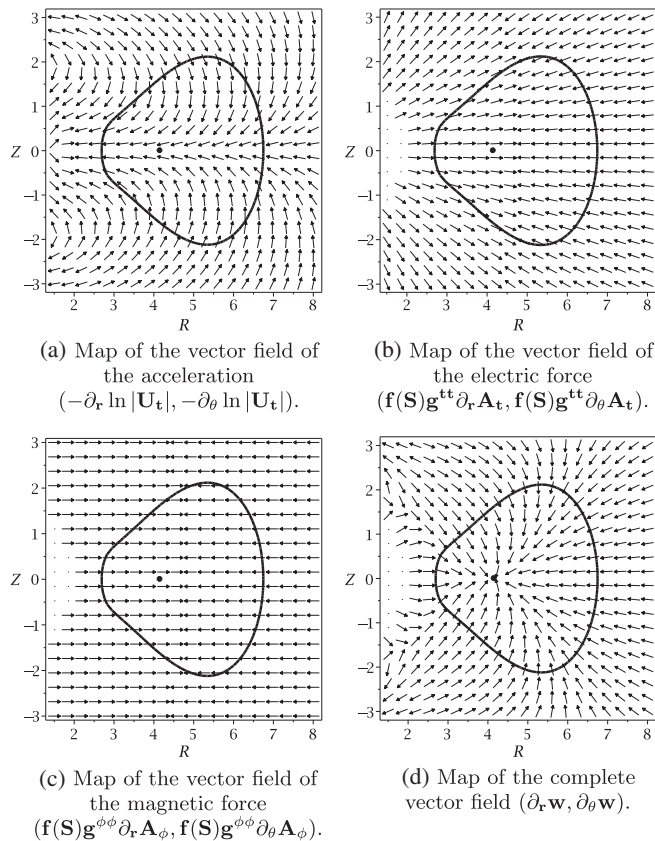


FIG. 11. Maps of the vectors field, in cylindrical coordinates (R, Z) for the bound fluid structure presented in Fig. 7. In every plot the thick black line corresponds to a closed equipotential surface. The size of the arrows are fixed and does not represent the strength of each term.

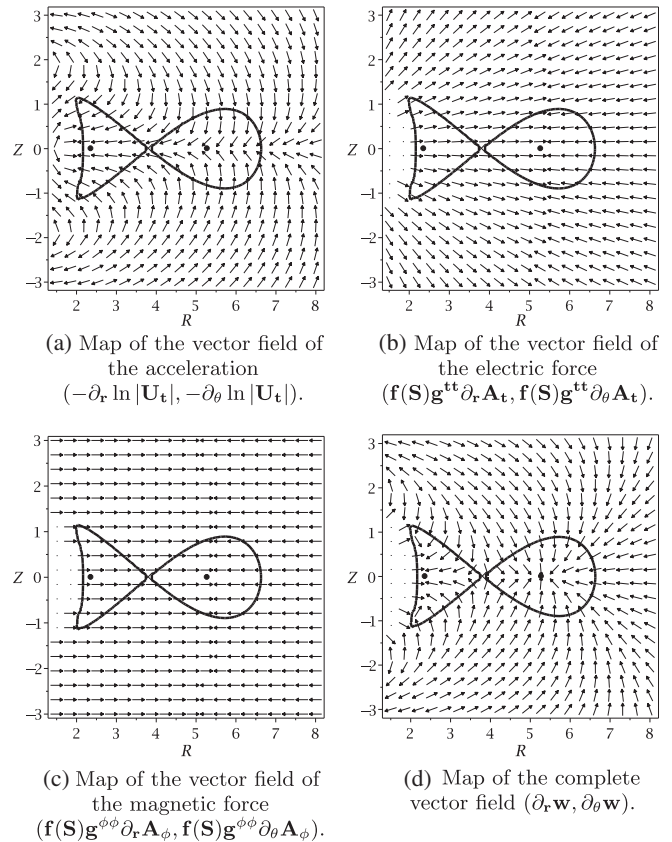


FIG. 12. Maps of the vectors field, in cylindrical coordinates (R, Z) , of the double tori presented in Fig. 8. In every plot the thick black line corresponds to the equipotential surface of the cusp equipotential. The size of the arrows are fixed and does not represent the strength of each term.

force points to the direction of the three points of interest, the two pressure maxima, and the cusp point. Except in the equatorial plane, where the flow is escaping the cusp point to go in the direction of one of the pressure maximum.

B. Influence of the parameter e on the cusps and pressure maximum

It is also interesting to see the influence of the parameter e on the position of the cusps and maxima of pressure in certain interesting configurations. One of them is depicted in Fig. 9; it is composed of two cusps points surrounding a bound fluid structure. We fix the following parameters to the values: $k_0 = 0.0001$ and $\ell = 15$, and then vary the value of e , from -10 to 30 . The result is shown in Fig. 13. We find the following different behavior.

- (i) The inner cusp: increasing the value of e tends to move the inner cusp inward, closer to the black hole, until a certain value of e is reached. At this point, the cusp starts to move outward for increasing e , further away from the black hole.
- (ii) For the pressure maximum, the behavior is opposite. For increasing values of e it is pushed away from the

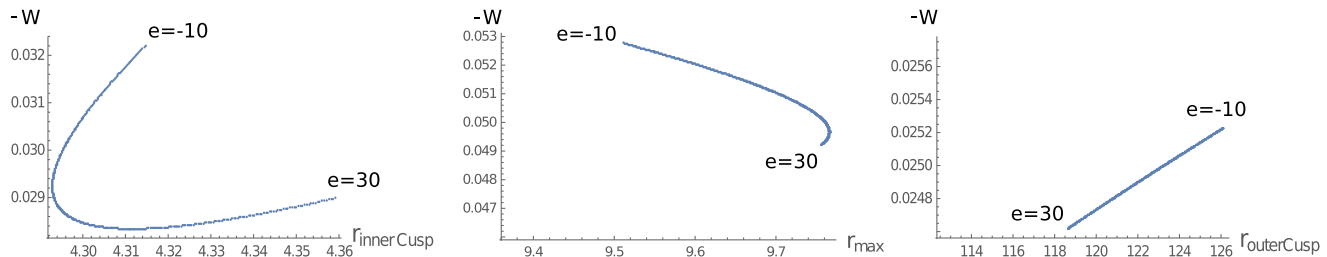


FIG. 13. From the left to the right: Variation of the radius of the inner cusp, the pressure maximum of the bound fluid structure and the outer cusp for $k_0 = 0.0001$, $\ell = \sqrt{15}$ and various values of e . For $e = 10$ the related configuration is shown in Fig. 9.

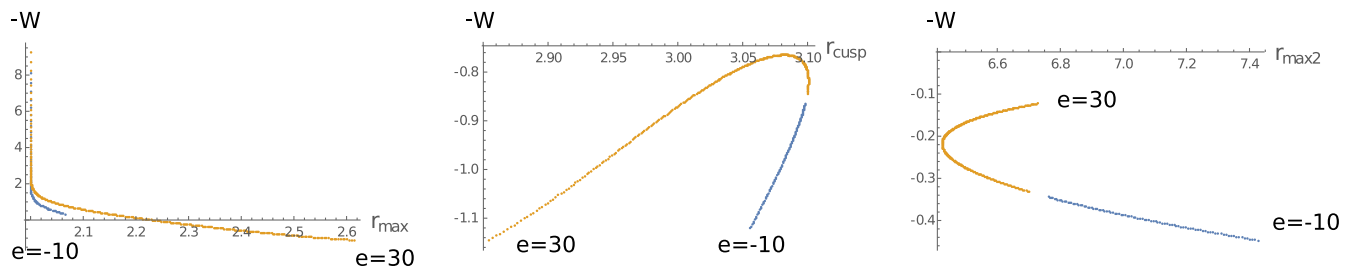


FIG. 14. From the left to the right: Variation of the pressure maximum of the inner bound fluid structure, of the cusp and the pressure maximum of the second bound structure, for $k_0 = -0.006$, $\ell = 5$ and various values of e . These parameter sets are related to configurations with potentials that have the same qualitative shape as the one pictured in Fig. 8.

black hole, until a certain value of e is reached. It then starts to move inward.

- (iii) The outer cusp: Its radius is moving inward when the value of e is increasing.

Another interesting configuration is the double tori one (see Fig. 14). In the case when e approaches 0, the inner bound solution approaches the horizon, then it is tricky to compute the configuration. Therefore, we vary e from -10 to -0.4 and from 1 to 30 (see Fig. 14). The variations exhibit, as above, various behavior.

- (i) For the radius of the inner pressure maximum, we notice that for increasing values of e , the radius moves outward. For smaller values of e , solutions approach the horizon, until the solution disappears.
- (ii) The cusp point: A similar behavior compared to the previous case is found. The cusp moves outward for an increasing value of e . At a certain value of e it starts to go back inward.
- (iii) For the radius of the outer pressure maximum, we see that the behavior is the opposite of the one of the cusp point.

In the case of a bound fluid structure only, as depicted in Fig. 7, the variation of the radius of the pressure maximum is close to the one shown for the inner maximum of the double tori solution, except that it can be pushed further outward.

VII. CONCLUSION

In this paper, we have presented a relativistic description of an electrically charged fluid in circular motion surrounding a

static black hole. The system is embedded in an electric field induced from the uniform magnetic field and a large scale asymptotically uniform magnetic field. Both the fields are the test ones and do not influence the spacetime; the electric and magnetic fields produced by the charged fluid are neglected. We showed that in the special case of constant specific angular momentum, we succeeded to construct the effective potential and built the equipotential surfaces. This effective potential shows various behavior leading to the existence of bound fluid structures in the equatorial plane. Those bound structures can appear with or without cusp points (inner or outer point). We found that equilibrium solutions of two bound fluid structures linked by a cusp can exist. Moreover, we succeeded to constrain the values of the model parameters (k_0, ℓ) , and to know by choosing a fixed value of e and n , which behavior exhibits the effective potential by using bifurcation theory. Also, we have shown that even if both the electric and the magnetic fields do not influence the spacetime, they have an impact on the existence of the equilibrium solutions. By varying the parameter e , we showed that the bifurcation set changes, meaning for a fixed value of (k_0, ℓ) , the behavior of the potential can exhibit different forms. The configuration of the solutions will then be different. We went further by studying the vector fields of each part (acceleration, electric force and magnetic force separately). We found some expected behaviors as the direction of the field due to the magnetic force, the radial behavior of the force due to the electric field and finally the attraction of the pressure maximum and the cusp point. All vectors point in the direction of these two particular points, except in the equatorial plane, where they escape from the cusp point.

One of the interesting results is that both the electric and magnetic vector fields change sign through the fluid at the same radius. We have also shown that the vertical extension in the outer part is due to the strength of the electric field which counteracts the effect due to the acceleration. In the inner part, the effect is the opposite. The acceleration is stronger than the electric part and make the shape thinner. Finally, we showed how the radius of the inner and outer cusp points and the one of the pressure maximum vary for a fixed (k_0, n, ℓ) in function of e .

We can conclude that external fields like electric and magnetic fields have a clear effect on the shape of the fluid structure, but also on the behavior of the effective potential. In this work, the specific charge density is set arbitrary, and the model highly depends on it. We have to remind that all the results shown in the paper are valid for the specific form

of q that we have chosen. This point has to be improved, to find more realistic specific charged profiles and is the subject of ongoing work.

ACKNOWLEDGMENTS

A. T. and E. H. acknowledge support from the Research Training Group 1620 “Models of Gravity” funded by the German Science Foundation DFG. E. H. is also grateful for support from the DFG funded Center of Excellence EXC 2123 “QuantumFrontiers.” V. K., K. S. and J. K. acknowledge Czech Science Foundation collaboration project (GAČR 19-01137J). J. K. and P. S. would like to express their acknowledgment for the support of the Research Centre for Theoretical Physics and Astrophysics, Institute of Physics, Silesian University in Opava.

-
- [1] B. Punsly, *Black Hole Gravitohydromagnetics* (Springer, New York, 2008), Vol. 355.
 - [2] C. Palenzuela, L. Lehner, O. Reula, and L. Rezzolla, Beyond ideal MHD: Towards a more realistic modelling of relativistic astrophysical plasmas, *Mon. Not. R. Astron. Soc.* **394**, 1727 (2009).
 - [3] L. Rezzolla and O. Zanotti, *Relativistic Hydrodynamics*, edited by L. Rezzolla and O. Zanotti (Oxford University Press, New York, 2013), ISBN-10: 0198528906, ISBN-13: 978-0198528906.
 - [4] J. Frank, A. King, and D. J. Raine, *Accretion Power in Astrophysics*, by Juhan Frank and Andrew King and Derek Raine (Cambridge University Press, Cambridge, England, 2002), pp. 398, ISBN 0521620538.
 - [5] F. Yuan and R. Narayan, Hot accretion flows around black holes, *Annu. Rev. Astron. Astrophys.* **52**, 529 (2014).
 - [6] M. Abramowicz, M. Jaroszynski, and M. Sikora, Relativistic, accreting disks, *Astron. Astrophys.* **63**, 221 (1978).
 - [7] M. Kozłowski, M. Jaroszynski, and M. A. Abramowicz, The analytic theory of fluid disks orbiting the Kerr black hole, *Astron. Astrophys.* **63**, 209 (1978).
 - [8] J. A. Font and F. Daigne, The runaway instability of thick discs around black holes—I. The constant angular momentum case, *Mon. Not. R. Astron. Soc.* **334**, 383 (2002).
 - [9] L. Rezzolla, O. Zanotti, and J. A. Font, Dynamics of thick discs around Schwarzschild-de Sitter black holes, *Astron. Astrophys.* **412**, 603 (2003).
 - [10] P. Slaný and Z. Stuchlík, Relativistic thick discs in the Kerr de Sitter backgrounds, *Classical Quantum Gravity* **22**, 3623 (2005).
 - [11] H. Kucáková, P. Slaný, and Z. Stuchlík, Toroidal configurations of perfect fluid in the Reissner-Nordström-(anti)-de Sitter spacetimes, *J. Cosmol. Astropart. Phys.* **01** (2011) 033.
 - [12] D. Pugliese, G. Montani, and M. G. Bernardini, On the Polish doughnut accretion disc via the effective potential approach, *Mon. Not. R. Astron. Soc.* **428**, 952 (2013).
 - [13] S. S. Komissarov, Magnetized tori around Kerr black holes: Analytic solutions with a toroidal magnetic field, *Mon. Not. R. Astron. Soc.* **368**, 993 (2006).
 - [14] S. Gimeno-Soler and J. A. Font, Magnetised Polish doughnuts revisited, *Astron. Astrophys.* **607**, A68 (2017).
 - [15] P. Mach, S. Gimeno-Soler, J. A. Font, A. Odrzywólek, and M. Piróg, Self-gravitating magnetized tori around black holes in general relativity, *Phys. Rev. D* **99**, 104063 (2019).
 - [16] J. C. Weingartner, B. T. Draine, and D. K. Barr, Photoelectric emission from dust grains exposed to extreme ultraviolet and X-ray radiation, *Astrophys. J.* **645**, 1188 (2006).
 - [17] B. T. Draine and E. E. Salpeter, On the physics of dust grains in hot gas, *Astrophys. J.* **231**, 77 (1979).
 - [18] D. A. Mendis and M. Rosenberg, Cosmic dusty plasmas, *Annu. Rev. Astron. Astrophys.* **32**, 419 (1994).
 - [19] A. Tiengo, P. Esposito, S. Mereghetti, R. Turolla, L. Nobili, F. Gastaldello, D. Götz, G. L. Israel, N. Rea, L. Stella, S. Zane, and G. F. Bignami, A variable absorption feature in the X-ray spectrum of a magnetar, *Nature (London)* **500**, 312 (2013).
 - [20] J. Kovář, P. Slaný, Z. Stuchlík, V. Karas, C. Cremaschini, and J. C. Miller, Role of electric charge in shaping equilibrium configurations of fluid tori encircling black holes, *Phys. Rev. D* **84**, 084002 (2011).
 - [21] J. Kovář, P. Slaný, C. Cremaschini, Z. Stuchlík, V. Karas, and A. Trova, Electrically charged matter in rigid rotation around magnetized black hole, *Phys. Rev. D* **90**, 044029 (2014).
 - [22] J. Kovář, P. Slaný, C. Cremaschini, Z. Stuchlík, V. Karas, and A. Trova, Charged perfect fluid tori in strong central gravitational and dipolar magnetic fields, *Phys. Rev. D* **93**, 124055 (2016).
 - [23] K. Schrovén, A. Trova, E. Hackmann, and C. Lämmerzahl, Charged fluid structures around a rotating compact object

- with a magnetic dipole field, *Phys. Rev. D* **98**, 023017 (2018).
- [24] A. Trova, K. Schroven, E. Hackmann, V. Karas, J. Kovář, and P. Slaný, Equilibrium configurations of a charged fluid around a Kerr black hole, *Phys. Rev. D* **97**, 104019 (2018).
- [25] The weak-field limit of this charged fluid model was also introduced [26,27].
- [26] A. Trova, V. Karas, P. Slaný, and J. Kovář, Electrically charged matter in permanent rotation around magnetized black holes: a toy model for self-gravitating fluid Tori, *Astrophys. J. Suppl. Ser.* **226**, 12 (2016).
- [27] P. Slaný, J. Kovář, Z. Stuchlík, and V. Karas, Charged Tori in spherical gravitational and dipolar magnetic fields, *Astrophys. J. Suppl. Ser.* **205**, 3 (2013).
- [28] R. M. Wald, Black hole in a uniform magnetic field, *Phys. Rev. D* **10**, 1680 (1974).
- [29] M. Azreg-Ainou, Vacuum and nonvacuum black holes in a uniform magnetic field, *Eur. Phys. J. C* **76**, 414 (2016).
- [30] J. P. Ostriker and J. W.-K. Mark, Rapidly rotating stars. I. The self-consistent-field method, *Astrophys. J.* **151**, 1075 (1968).
- [31] Y. Tomimura and Y. Eriguchi, A new numerical scheme for structures of rotating magnetic stars, *Mon. Not. R. Astron. Soc.* **359**, 1117 (2005).
- [32] J. Otani, R. Takahashi, and Y. Eriguchi, Equilibrium states of magnetized toroid-central compact object systems, *Mon. Not. R. Astron. Soc.* **396**, 2152 (2009).
- [33] Z. Stuchlík, M. Kološ, J. Kovář, P. Slaný, and A. Tursunov, Influence of cosmic repulsion and magnetic fields on accretion disks rotating around Kerr black holes, *Universe* **6**, 26 (2020).
- [34] R. Thom, The two-fold way of catastrophe theory, *Lect. Notes Math.* **525**, 235 (1976).
- [35] E. C. Zeeman, *Catastrophe Theory. Selected Papers, 1972–1977* (Addison-Wesley Publishing Company, Reading, Massachusetts, 1977), p. 675.
- [36] R. Thom, Catastrophe theory and its applications, *Proc. 7th nat. Math. Conf., Tabriz 1976* (Society for Industrial and Applied Mathematics, 1977), pp. 372–379.
- [37] M. Golubitsky, An introduction to catastrophe theory and its applications, *Siam Rev.* **20**, 352(1978)..
- [38] V. I. Arnold, *Catastrophe theory* (Springer-Verlag, Berlin, 1984), pp. iv+79, translated from the Russian by R. K. Thomas.